IUTAM Conference on Deformation and Failure of Granular Materials / Delft / 31 Aug. – 3 Sept. 1982

Computer implementation of a double-hardening model for sand

D.V.GRIFFITHS & I.M.SMITH
University of Manchester, UK

F.MOLENKAMP
Delft Soil Mechanics Laboratory, Netherlands

1 INTRODUCTION

Arguably, rational attempts to formulate realistic stress-strain relations for granular material began with the Cam-clay (Roscoe et al 1958; Roscoe and Burland 1968) and stress-dilatancy (Rowe 1962, 1971) theories. These were initially aimed at an understanding of the material's behaviour but as computing power has increased, have subsequently been used to predict stress-strain behaviour of soils in boundary value problems. If this is the aim, two factors are closely linked - firstly the degree of complexity of the soil "model" in relation to the problem at hand, and secondly whether the resulting behaviour can be computed at all (at reasonable cost) using present technology and numerical analysis skills.

Therefore the theme of the present paper is this interrelationship - a constitutive model of "sufficient" complexity and its computability in boundary value problems where the use of a complicated soil model is really justified.

The three basic features of granular material behaviour which constitutive laws seek to model are stiffness, strength and volume change (porewater pressure) and the last of these is the most difficult to describe. However, in many cases accurate volume change prediction may not be necessary. Undrained clays deform with zero volume change and can be treated quite satisfactorily as elastic-perfectly plastic solids (Smith and Hobbs 1974). Similarly for many drained c-ϕ soils in relatively unconfined situations (slopes, retaining walls, shallow footings) the degree of volume change prior to and at failure can be shown to be of minor importance (Zienkiewicz et al 1975; Griffiths 1980), to the description in a global sense of load-deformation up to collapse. Therefore an elastic-Mohr Coulomb plastic analysis could well suffice.

However there are situations where neglecting to take into account the true contractive/dilative volume change behaviour of soil could not lead to an adequate modelling of real behaviour. Examples are:

1. Static liquefaction of loose, undrained sands where small movements trigger off porewater pressure increases leading to small effective stresses and fluidisation.

2. Stress redistribution behind flexible bulkheads retaining dense sands. Again small movements are enough to trigger off volume changes which cause major redistribution of passive pressures near the top of the wall. Bending moments can be doubled and lead to structural yield.

3. Lateral loads on structures adjacent to footings. Whereas it may be possible to fit the load-deflection behaviour of an isolated footing quite well with a simple model, the erroneous volume changes will imply erroneous lateral transfer of load to any adjacent buried structure.

4. Piles in sand. Crushing at the pile tip is accentuated by the difficulty any failure mechanism has in forming. Thus a good description of compressibility is vital to an understanding of this deformation problem.

5. Dredging of undrained sands. Here dilatancy governs the onset of cavitation or critical confinement and hence the forces applicable to dredging blades.

The framework within which most models of soil behaviour, including the present one, are described is the theory of plasticity. Early calculations of simple

boundary value problems using the stress-dilatancy and Cam-clay models were reported by Smith (1970,1971). These involved a single yield/potential function of the deviatoric type although Smith (1971) suggested that the effects of deviatoric and volumetric yield could be combined in a single surface. However, later authors (Lade 1977; Vermeer 1980) introduced "double hardening" models in which separate functions describe deviatoric and volumetric behaviour. (This had actually been done earlier in "revised modified Cam clay" - Roscoe and Burland 1968). The model described in the present paper is also of this type and makes use of Lade's and Vermeer's work. However, although some additions and alterations have been made, the essential features of the discussion apply to any double hardening model. Despite the usage of this double-hardening model the authors believe that still some coupling will exist between the plastic volume changes in deviatoric and isotropic loading, but at present insufficient insight in this coupling phenomenon exists to take this into account properly.

Quite apart from the complexity of the model itself lies the difficulty of its numerical implementation. The extreme nonlinearity of the stress-strain behaviour requires an incremental approach, possibly with additional iterations within each step to satisfy the yield criteria. Later in the paper the sensitivity of calculation speed to stress path traversed will be emphasised.

2 BRIEF DESCRIPTION OF PRESENT MODEL

(For more detail, see Molenkamp (1981)).

The following symbols will be used:

$v = \frac{\varepsilon_{ij}\delta_{ij}}{\sqrt{3}}$ isotropic strain component in principal strain space

$s = \frac{\sigma_{ij}\delta_{ij}}{\sqrt{3}}$ isotropic stress component in principal stress space

$\gamma = \sqrt{e_{ij}e_{ij}}$ deviatoric strain component in principal strain space

$t = \sqrt{s_{ij}s_{ij}}$ deviatoric stress component in principal stress space.

In the above

$e_{ij} = \varepsilon_{ij} - \frac{e_{kl}\delta_{kl}}{3}\delta_{ij}$ deviatoric strain tensor

$s_{ij} = \sigma_{ij} - \frac{\sigma_{kl}\delta_{kl}}{3}\delta_{ij}$ deviatoric stress tensor

and

$$\gamma = \left[\left(\tfrac{1}{3}\left((\varepsilon_{11}-\varepsilon_{22})^2+(\varepsilon_{22}-\varepsilon_{33})^2+(\varepsilon_{33}-\varepsilon_{11})^2\right)+2(\varepsilon_{12}^2+\varepsilon_{23}^2+\varepsilon_{31}^2)\right)\right]^{\frac{1}{2}}$$

$$t = \left[\left(\tfrac{1}{3}\left((\sigma_{11}-\sigma_{22})^2+(\sigma_{22}-\sigma_{33})^2+(\sigma_{33}-\sigma_{11})^2\right)+2(\sigma_{12}^2+\sigma_{23}^2+\sigma_{31}^2)\right)\right]^{\frac{1}{2}}.$$

Thus the model is defined in terms of invariants. In its full form it requires 21 (essentially dimensionless) parameters for its definition, but as will be described later this number could easily be reduced to 10 or even 3 in the absence of highly detailed experimental observations.

The response of soil to load being nonlinear, the parameters are found by fitting best curves to the results of experimental data. At present, the basis of the curve fits is the work of Rowe (1962,1971), Tatsuoka and Ishihara (1974), Lade and Duncan (1975), Lade (1977), Yamada and Ishihara (1979) and Vermeer (1980).

Increments of strain are split into three components: elastic, isotropic plastic and deviatoric plastic. The numbers of parameters required to describe these are in the ratio 3:2:16 which partly reflects the lack of detailed knowledge about the first two components but also reflects the complexity and importance of shear-dilatancy coupling in soil. The three components will now be described.

3 NONLINEAR ELASTIC COMPONENT

An isotropic nonlinear elastic model is adopted, following Vermeer (1980). This takes the form

$$\varepsilon_{ij}^e = \frac{1}{2\mu}\left(\delta_{ik}\delta_{jl} - \frac{\nu}{1+\nu}\delta_{ij}\delta_{kl}\right)\sigma_{kl} = \frac{A_{ijkl}\sigma_{kl}}{2\mu}$$

in which

$\mu = \mu_o\left(\frac{\sigma}{p_a}\right)^{n_v}$

$\sigma = \frac{s}{\sqrt{3}}\sqrt{\left(1+\frac{(1+\nu)}{(1-2\nu)}\frac{t^2}{s^2}\right)}$

p_a = atmospheric pressure

n_v = parameter

ν = Poisson's ratio (assumed constant).

In an unloading test at $t/s = 0$, the volumetric behaviour becomes

$$v^e = A\left(\frac{s}{p_a}\right)^{AP}$$

where A and AP $(= 1-n_v)$ are dimensionless parameters. The power AP theoretically lies between $\frac{1}{3}$ and $\frac{1}{2}$ (Rowe 1971) and both Rowe and Lade (1977) quote a value of 0.42 for quartz sand. Similarly ν is probably in the range 0.1 to 0.3 and in the absence of detailed knowledge, 0.2 could be used. The final parameter A remains to be found by fitting and for Lade's (1977) data lies in the range 0.001 to 0.002.

4 PLASTIC COMPRESSIVE COMPONENT

Pending better data the spherical "cap" used by Lade (1977) has been adopted. In this model the yield surface $F_c = 0$ and plastic potential $G_c = 0$ coincide, forming spheres in principal stress space, centred at the origin.

With the usual definition of invariants, the spheres have equations

$$F_c = G_c = I_1^2 + 2\,I_2^2 - f_c = 0$$

such that their radius is $\sqrt{f_c}$.

The plastic strain components are given by

$$d\varepsilon_{ij}^c = \frac{\frac{\partial G_c}{\partial \sigma_{ij}} \frac{\partial F_c}{\partial \sigma_{kl}} d\sigma_{kl}}{H_c}$$

in which H_c is the hardening parameter. From loading/unloading tests at constant t/s the plastic isotropic compression v^c can be written

$$v^c = B\left(\frac{s}{p_a}\right)^{BP}$$

where B and BP are parameters which are related to hardening:

$$H_c = \frac{4\,p_a^3}{B.BP}\left(\frac{f_c}{p_a^2}\right)^{\frac{3-BP}{2}}$$

The power BP seems to be of the order of 0.7 (Lade 1977).

5 PLASTIC DEVIATORIC COMPONENT

Here the difficulty of curve fitting intensifies and typical results are shown for t–s space in Figure 1. Both yield and failure surfaces are based on the data of Tatsuoka and Ishihara (1974) and are assumed to be of the form

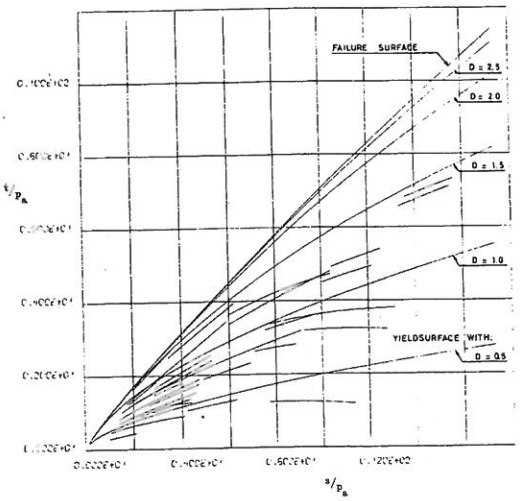

YIELDSURFACES OF LOOSE FUJI SAND AS MEASURED BY TATSUOKA, ISHIHARA (1974).

Fig.1

$$t_f = p_a.C.\left(\frac{s}{p_a}\right)^{CP} \quad \text{for failure,}$$

where C and CP are parameters and

$$t_y = p_a.D.\left(\frac{s}{p_a}\right)^{DP} \quad \text{for yield.}$$

Parameters CP and SP reflect the curvatures of failure and yield surfaces respectively so that if $CP = 1$ (straight failure surface) then C is analogous to ϕ, a peak angle of friction where

$$\phi = \arcsin\left(\frac{3C}{2\sqrt{2}+C}\right).$$

An extra parameter n controls the curvature of the yield surfaces near failure.

In the π-plane the authors adopt Lade and Duncan's (1975) failure surfaces which take the form

$$F_d = \frac{I_1^3}{I_3} - 27 - f_d = 0$$

and are shown in Figure 2 compared with Mohr-Coulomb.

5.1 Plastic potentials

In the deviatoric plane, Rowe's (1962, 1971) stress-dilatancy theory is adopted. In a refined approach the mobilised angle of friction, ϕ_f, can be related to the constants ϕ_μ and ϕ_{cv} as shown in Figure 3, but in a rougher study, ϕ_f

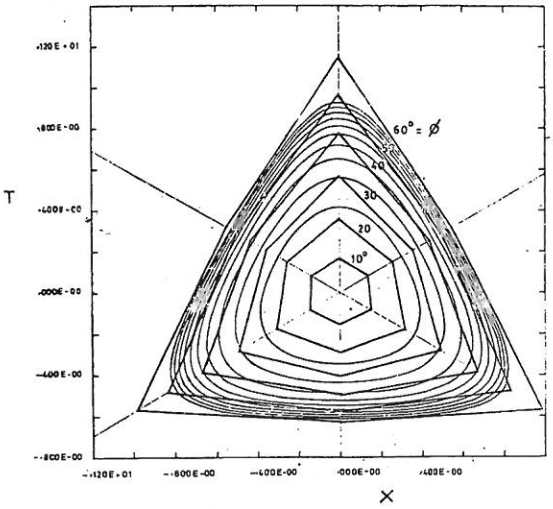

INTERSECTION OF LADE'S YIELDSURFACES FOR DENSE SACRAMENTO RIVER SAND

Fig.2

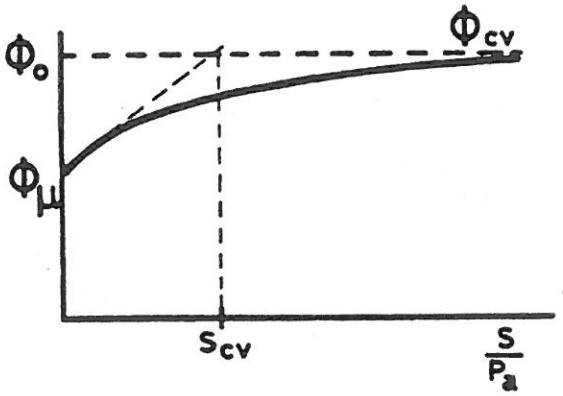

Fig.3 Dependence of ϕ_f on s.

could be set to ϕ_μ and SCV assigned a large value. In addition, a modification can be made to Rowe's potentials at low stress ratios t/s. This involves three extra parameters, NU, VGC and VGP, but again in a rough approach VGP could be set to 0 and VGC to 1 to recover basic stress-dilatancy.

In the π-plane, fits are made to the results of true triaxial tests reported by Yamada and Ishihara (1979). This involves three parameters CG, CV and RT. The potentials have a similar general shape to those of Lade and Duncan (1975) but have more rounded corners. For example, RT = 1 recovers Lade, RT = 0^+ would describe circles whereas RT = 0.3 produced the best fit to the true triaxial data used.

5.2 Hardening

The final few parameters relate to deviatoric hardening and so have a direct influence on the magnitudes of plastic strain increments rather than their ratios. They can therefore be expected to vary much more widely with soil density.

Since $d\varepsilon^d_{ij} = \lambda \frac{\partial G_d}{\partial \sigma_{ij}} = \frac{\frac{\partial G_d}{\partial \sigma_{ij}} \frac{\partial F_d}{\partial \sigma_{kl}} d\sigma_{kl}}{H_d}$

the hardening H_d may be written

$$H_d = \frac{\frac{\partial F_d}{\partial \sigma_{kl}} d\sigma_{kl}}{\lambda} .$$

Experiments by Yamada and Ishihara (1979) relate the equivalent shear strain γ^d_{eq} in triaxial compression tests at constant s to the stress ratio by:

$$\gamma^d_{eq} = E\left(\frac{t}{s}\right)^{EP} \left(\frac{s}{p_a}\right)^{LB}$$

where E, EP and LB are parameters, of which E is much the most sensitive. Typical values of EP and LB have been found to be 2 and 0.3 respectively. The parameter n (relatively insensitive) governs also deviation from the above behaviour close to failure.

6 SUMMARY OF MODEL PROPERTIES AND THEIR DETERMINATION

Figures in parentheses indicate constant values applicable in a rough approach for quartz sand.

a. Nonlinear Elastic Component
   - ν Poisson's ratio (0.2)
   - AP Power of law (0.42)
   - A Modulus

b. Plastic Compressive Component
   - BP Power of law (0.7)
   - B Modulus

c. Plastic Deviatoric Component
   - i. Yield and failure
     - CP Curvature of failure surface (1)

C Related to the peak friction angle - ϕ

DP Curvature of yield surfaces (0.6)

ii. Plastic potentials

1. Deviatoric plane

ϕ_μ Angle of mineral friction (27^o)

ϕ_{cv} Friction angle at constant volume (34^o)

SCV Adjustment to ϕ_f (200)

VGC, VGP, NU } Modifications to stress-dilatancy at low stress ratios (1), (0), (1)

2. π-Plane

CG, CV, RT } Modifications to Lade/Duncan potentials (0.8), (0.8), (0.3)

3. Hardening

E Modulus

EP Power of stress ratio (2)

LB Power of mean stress (0.3)

N Adjustment close to failure (7)

Thus the moduli A, B and E are the main variables, which, since they relate strains to stresses, increase with increasing void ratio. They are to be obtained from the results of drained triaxial tests following specific stress paths.

7 IMPLEMENTATION USING FINITE ELEMENTS

7.1 Soil element tests

Most analyses were performed for stress-controlled paths so that the region of stress space being traversed was known in advance (Figure 4).

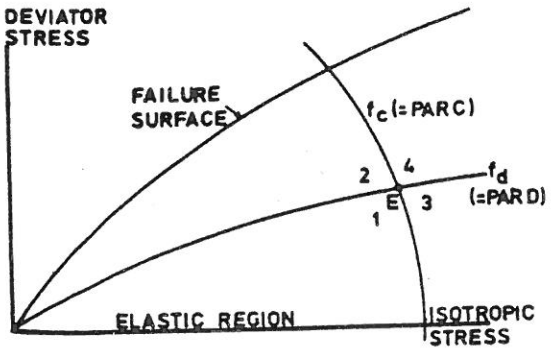

Fig.4 Four regions of stress space.

The tangent $\underline{D}$ matrix could therefore be computed and a simple Euler method was used, based on the average $\underline{D}$ over the stress increment (tangent stiffness, no iterative corrections). The steps could be taken small enough for the $\underline{D}$ at the start of the increment to be equally appropriate. For the (axisymmetric) element integration and programming details, see Smith (1982). Note that in general the $\underline{D}$ matrix and hence in this method the eventual stiffness matrix are unsymmetrical.

Figure 5 illustrates the typical performance of the elastic component of the model in isotropic loading and unloading, while Figure 6 illustrates the additional influence of the volumetric cap.

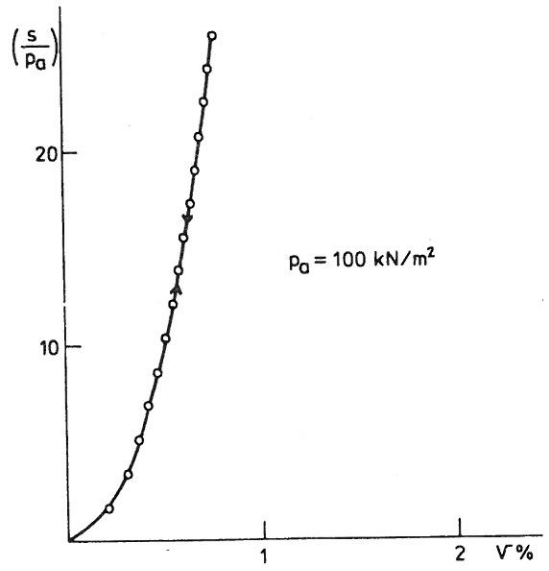

NON-LINEAR ELASTIC ISOTROPIC LOADING / UNLOADING

Fig.5

Turning to more general stress paths, Figure 7 shows a closed loop test involving phases of constant s and constant t loading and unloading. Figure 8 shows the response in terms of principal stress ratio $R = \sigma_1'/\sigma_3'$.

Figure 9 shows the effect of confining pressure on the results of constant s tests, illustrating the well known high friction angles associated with very low confining pressure. In terms of deviator stress, the specimen stiffens with increasing confinement while in terms of stress ratio it softens.

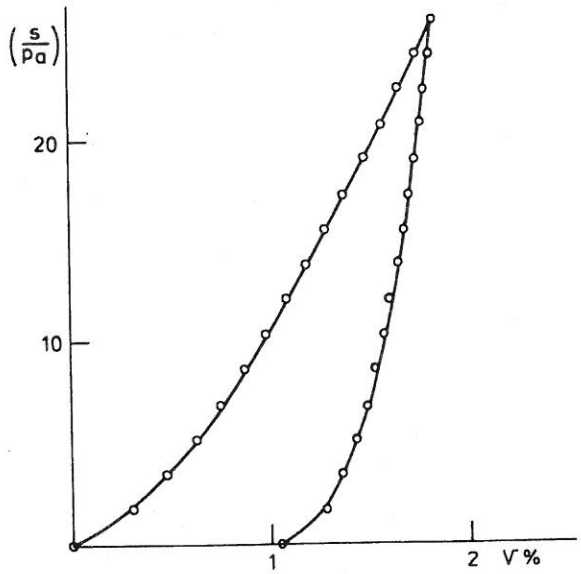

ISOTROPIC LOADING / UNLOADING INCLUDING CAP YIELD SURFACE

Fig.6

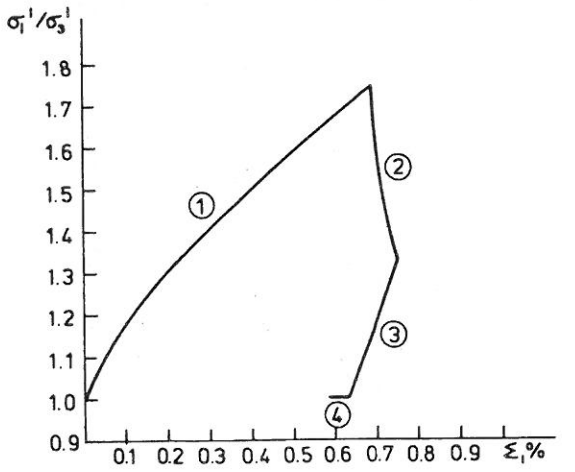

STRESS RATIO RESPONSE TO CLOSED LOOP

Fig.8

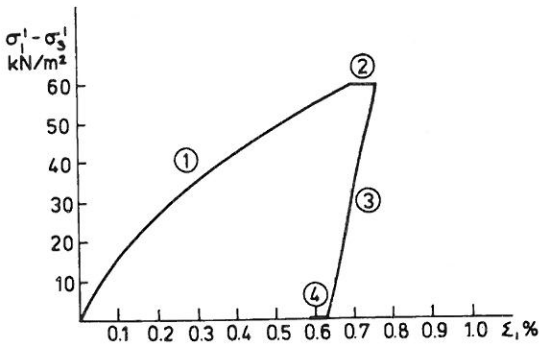

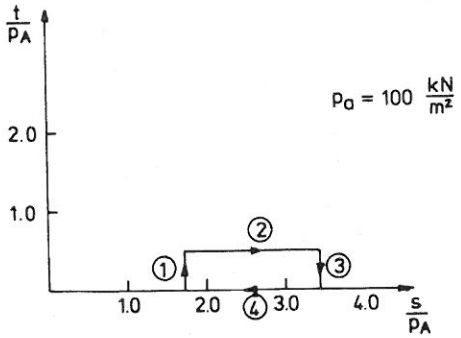

CLOSED LOOP STRESS PATH

Fig.7

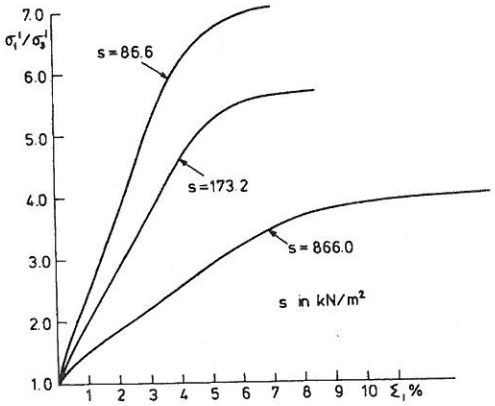

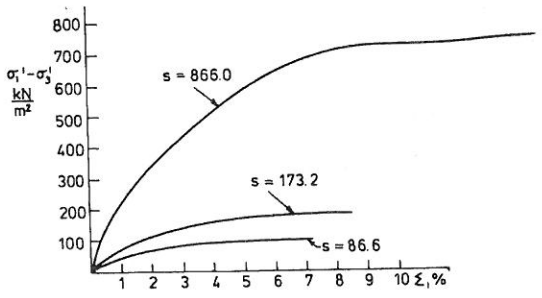

CONSTANT MEAN STRESS PATHS

Fig.9

Results of extension ("active"), constant s and compression ("passive") tests are shown in Figure 10, and a typically curved failure envelope in Figure 11.

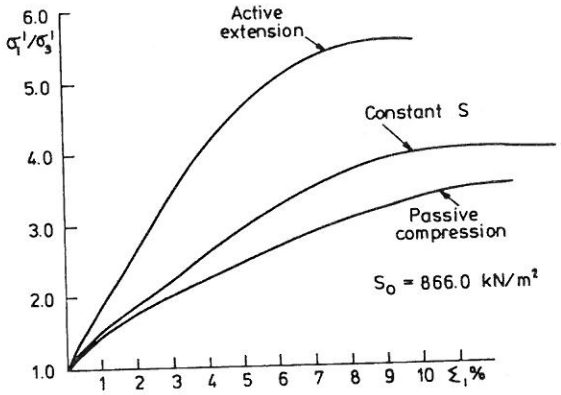

ACTIVE, PASSIVE AND CONSTANT S TESTS.

Fig.10

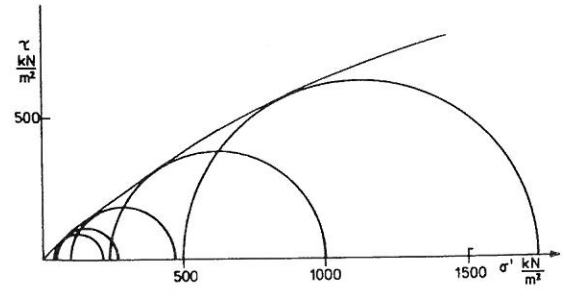

EFFECTIVE FAILURE ENVELOPE

Fig.11

In constant cell pressure tests, Figure 12, the failure stress ratio is significantly affected. Similarly, volume changes are shown in Figure 13, illustrating that at high cell pressure dilatancy is almost completely suppressed.

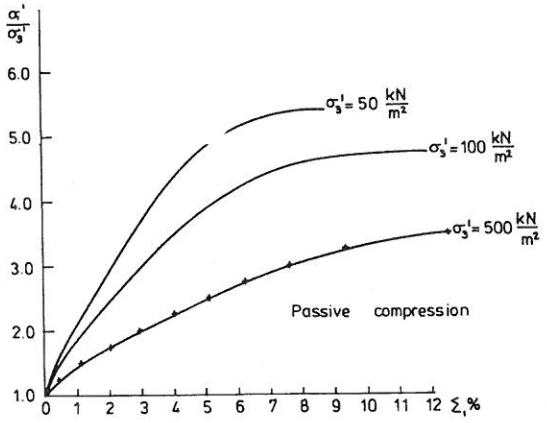

INFLUENCE OF CELL PRESSURE ON STRESS RATIO AT FAILURE

Fig.12

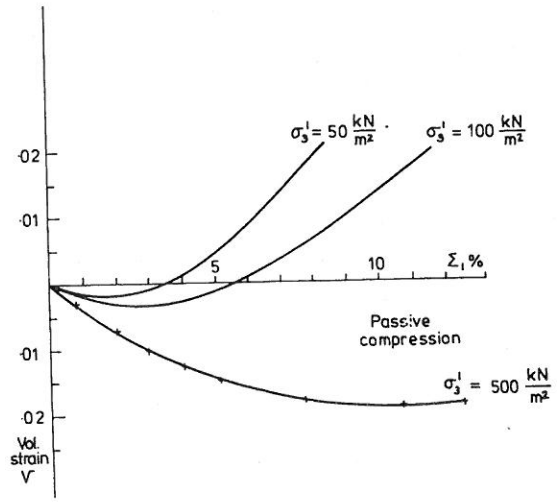

INFLUENCE OF CELL PRESSURE ON VOLUMETRIC STRAIN

Fig.13

When the results of tests at constant R are computed, Figure 14, the results are in remarkably good agreement with those of Rowe (1971) - Figure 2.17b. Compressive loading at high R actually causes dilation due to the specimen's induced structure.

Results from an undrained test at constant cell pressure are shown in

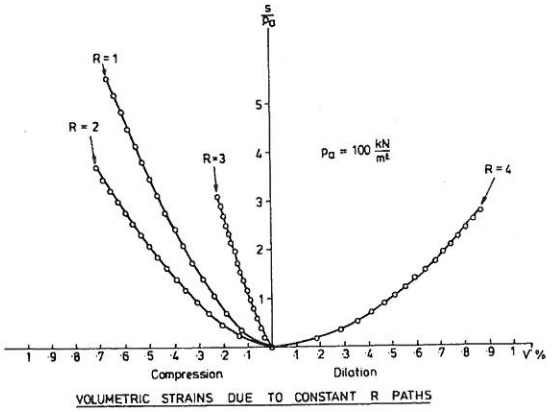

VOLUMETRIC STRAINS DUE TO CONSTANT R PATHS

Fig.14

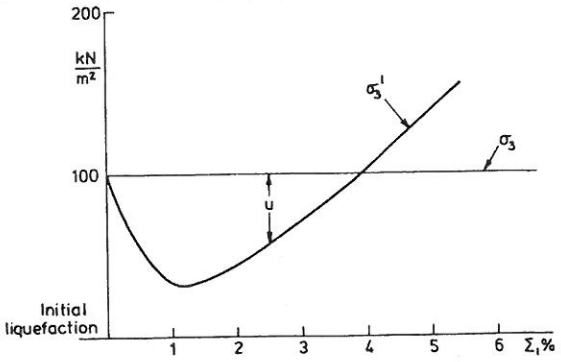

EFFECTIVE AND TOTAL RADIAL STRESSES (UNDRAINED)

Fig.16

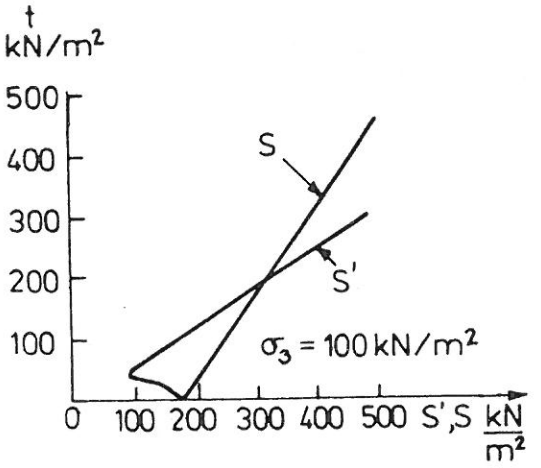

EFFECTIVE AND TOTAL UNDRAINED STRESS PATHS

Fig.15

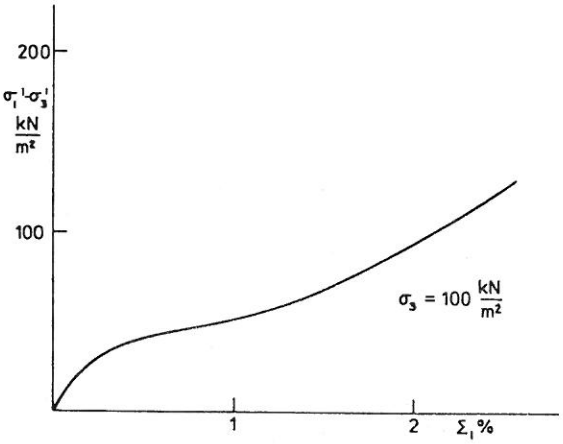

DEVIATOR STRESS VS. AXIAL STRAIN (UNDRAINED)

Fig.17

Figure 15. Note the strong curvature of the stress path in effective stress space. It was found that this path was very sensitive to calculation step size (as it is to membrane penetration - Molenkamp and Luger (1981)). Thus in Figures 16, the progress of the effective minor principal stress towards zero (initial liquefaction) will be sensitive to detailed calculation. The deviator stress in undrained loading, Figure 17 shows the familiar point of inflexion due to pore pressure variation and the general upward trend that continues until critical confinement or cavitation occurs.

The above results show, in very general terms, that the proposed model is capable of describing many essential features of the behaviour of drained and undrained soil.

7.2 Boundary value problems

In general problems, the direction of the stress increment within regions 1, 2, 3, 4, see Figure 4, is not known in advance. The authors begin with the assumption that the elastic constitutive model applies, and hence compute the stress increment. If this is incorrect, next the model appropriate to the region of the

computed increment is tried, and so on. If none of the four regions seems appropriate because the increment is partially elastic and partially plastic then the elastic assumption holds. For very low effective stresses, say s 1 N/m^2, an "air" or "water" element can be substituted. For stress probes directed outside the failure surface, projections along the failure surface are substituted.

However, bearing in mind the comments in the introduction, the use of such a model in the analyses of undrained boundary value problems will clearly prove to be expensive. The curvatures of the stress paths at various locations in the soil mass will be quite different and the idea of transformation of variables is clearly attractive. However, in a crude analysis, integration will proceed no faster than that of the slowest Gauss point. However some intriguing examples of potential liquefaction can be considered. Should ruptures propagate, the detailed conditions within the rupture planes appear to defy continuum calculations of the present kind.

8 CONCLUSIONS

Many of the special attributes of drained and undrained sands can be represented by double hardening models. A typical one has been outlined and its performance in various stress path tests examined. Special attention has been directed to a critical study of boundary value problems where the use of a complicated soil model is justified and the problems inherent in any large calculation using such a model.

9 REFERENCES

Griffiths, D.V. 1980. Finite element analysis of walls, footings and slopes. Ph.D. Thesis, Manchester University.

Lade, P.V. 1977. Elasto-plastic stress-strain theory for cohesionless soil with curved yield surfaces. Int. J. Solids Struct. 13:1019-1035.

Lade, P.V.& J.M. Duncan 1975. Elastoplastic stress-strain theory for cohesionless soils. J.Geotech.Eng.Div. ASCE. 107, FT10:1037-1053.

Molenkamp, F. 1981. Elasto-plastic double hardening model MONOT. Delft Soil Mechanics Laboratory Report.

Molenkamp, F.& H.J. Luger 1981. Modelling and minimisation of membrane penetration effects in tests on granular soils. Geotechnique 31, 4:471-486.

Roscoe, K.H., A.N. Schofield & C.P. Wroth 1958. On the yielding of soils. Geotechnique 8, 1:22-53.

Roscoe, K.H.& J.B. Burland 1968. On the generalised stress-strain behaviour of wet clays. Engineering Plasticity (eds Heyman, Leckie), Cambridge University Press, 535-609.

Rowe, P.W. 1962. The stress-dilatancy relation for static equilibrium of an assembly of particles in contact. Proc. Royal Soc. Series A, 269:500-527.

Rowe, P.W. 1971. Theoretical meaning and observed values of deformation parameters for soil. Proc. Roscoe Mem. Symp. Cambridge, 548-563.

Smith, I.M. 1970. Incremental numerical analysis of a simple deformation problem in soil mechanics. Geotechnique 20, 4:357-372.

Smith, I.M. 1971. Plane plastic deformation of soil. Stress-Strain Behaviour of Soils (ed. Parry), 548-563: Foulis.

Smith, I.M. 1982. Programming the finite element method, 351pp, Wiley.

Smith, I.M.& R. Hobbs 1974. Finite element analysis of centrifuged and built-up slopes. Geotechnique 24, 4:531-559.

Tatsuoka, F.& K. Ishihara 1974. Yielding of sand in triaxial compression. So ls and Foundations, 14, 2:63-76.

Vermeer, P.A. 1980. Formulation and analysis of sand deformation problems. Doctoral Thesis, Delft University of Technology, Netherlands.

Yamada, Y.& K. Ishihara 1979. Anisotropic deformation characteristics of sand under three dimensional stress conditions. Soils and Foundations, 19, 2:79-94.

Zienkiewicz, O.C., C. Humpheson & R.W. Lewis 1975. Associated and non-associated viscoplasticity and plasticity in soil mechanics. Geotechnique, 25, 4:671-689.